Competition between spin-glass and antiferromagnetic states in Tsai-type 1/1 and 2/1 quasicrystal approximants

Farid Labib [1,*] Hiroyuki Takakura,[2] Asuka Ishikawa,[3] and Ryuji Tamura [1]

[1]*Department of Material Science and Technology, Tokyo University of Science, Tokyo 125-8585, Japan*
[2]*Division of Applied Physics, Faculty of Engineering, Hokkaido University, Sapporo 060-8628, Japan*
[3]*Research Institute of Science and Technology, Tokyo University of Science, Tokyo 125-8585, Japan*

(Received 29 August 2022; revised 13 December 2022; accepted 15 December 2022; published 27 December 2022)

Systematic research was performed to investigate magnetic properties of the Tsai-type Ga-Pd-*RE* (*RE* = Gd, Tb, Dy, and Ho) systems, where both 1/1 and 2/1 quasicrystal approximants (ACs) are attainable at the same compositions as thermodynamical stable phases. Most of the samples exhibited spin-glass (SG)-like freezing behavior at low temperatures except Ga-Pd-Tb 2/1 AC and Ga-Pd-Ho 1/1 AC. The former showcased antiferromagnetic order at 5.78 K while the latter did not show any anomaly down to 1.8 K. Furthermore, 2/1 ACs were noticed to be less frustrated than their corresponding 1/1 ACs (based on the empirical rule of $|\theta_w/T_f|$) presumably due to the disorder-free environment in the nearest neighbor of the rare-earth sites that form a network of distorted octahedron in the 2/1 ACs. The spin dynamic in SG samples was also characterized by means of ac magnetic susceptibility measurements. The results evidenced a weak response of the freezing temperatures to the measurement frequency in the Heisenberg systems, i.e., Gd-contained ACs, in contrast to the non-Heisenberg systems, i.e., Tb-, Dy-, and Ho-contained ACs, where significant dependency is noticed for the latter. The spin-glass samples were further examined by fitting their freezing temperatures to the Vogel-Fulcher law.

DOI: 10.1103/PhysRevMaterials.6.124412

I. INTRODUCTION

Icosahedral quasicrystals (*i*QCs), as aperiodically ordered intermetallic compounds, generate sharp Bragg reflections with fivefold rotational symmetry indicating the presence of a long-range order without periodicity in their atomic configuration [1,2]. Their main structural building unit is a rhombic triacontahedron (RTH) cluster [3], which is a multishell polyhedron composed of four inner units (from the outermost one): an icosidodecahedron, an icosahedron, a dodecahedron, and a central unit, which is usually but not always a disordered tetrahedron. The rare-earth (*RE*) elements, as schematically shown in Fig. 1(a), typically occupy the vertices of the icosahedron shell. Approximant crystals (ACs), on the other hand, refer to periodic counterparts of the *i*QCs. The term "AC" is preceded by a rational approximation f_{n+1}/f_n of τ defined as $(1+\sqrt{5})/2$, where f_n denotes the nth Fibonacci number [2]. In this context, the higher the approximation we take, the more the structure resemblances to that of *i*QC [4]. Figures 1(b) and 1(c) represent the configuration of *RE* sites in the two lowest approximants, i.e., 1/1 and 2/1 ACs. Within one unit cell of 1/1 AC, as seen in Fig. 1(b), there exist 24 symmetrically equivalent *RE* sites [4], which increases to 104 sites with 5 different symmetries in the 2/1 AC [represented by spheres of different colors in Fig. 1(c)] [5,6]. Among these sites, RE_1-RE_4 belong to icosahedron vertices and four RE_5 dimers locate on the body-diagonal axes of acute rhombohedron (AR) units that fill the vacant space in between the RTH clusters. More details about structure parameters of *i*QC and their ACs can be found elsewhere [3].

As far as their magnetism is concerned, most of the Tsai-type *i*QCs and ACs reported to date showcase canonical spin-glass (SG)-like freezing behavior [7,8] while some exhibit long-range ferromagnetic (FM) [9–14], and antiferromagnetic (AFM) [15–20] order. So far, all the experimental efforts in developing stable *i*QCs with a long-range magnetic order, especially of an AFM type, have failed despite the claim of theoretical works, based on which no symmetry-related argument exists to prevent the establishment of long-range magnetic order in *i*QCs [21–27]. This suggests that the SG state in *i*QCs is induced by rather nonsymmetry-related parameters. One may consider structural defects such as chemical and/or positional disorders, random distribution of *RE*-*RE* distances, and the distribution of the easy axis or plane (in the non-Heisenberg members) as potential parameters that could provoke SG-like behavior in the *i*QCs [28]. The appearance of SG behavior in the binary Cd-Gd *i*QC [29], where neither chemical disorder nor magnetic anisotropy exist, suggests the distribution of *RE*-*RE* distances as a more dominant contributing factor to the spin-freezing phenomenon in *i*QCs. Quite recently though, a FM order has been discovered in rapidly quenched Au-Ga-Gd and Au-Ga-Tb *i*QCs providing the first experimental evidence of a long-range magnetic order in *i*QCs [14]. As a significant accomplishment, a correlation between electron concentration of the Tsai-type compounds (mostly Au-based) and their magnetic ground state has been proposed [9,10,17,20,30], based on which

*labib.farid@rs.tus.ac.jp

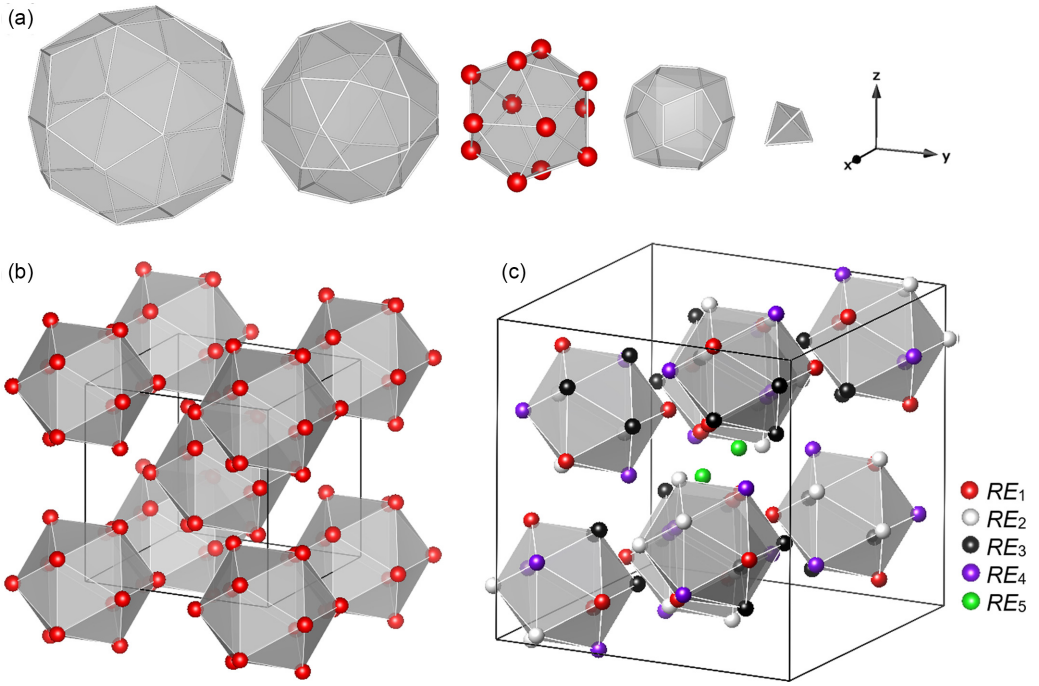

FIG. 1. (a) Typical shell structure of the main building unit in the Tsai-type icosahedral quasicrystals (*i*QCs). From left: a rhombic triacontahedron (RTH), an icosidodecahedron, an icosahedron, a dodecahedron, and a tetrahedron. Depending on the alloy system, the inner tetrahedron could be either ordered or disordered. The *RE* occupies the vertices of the icosahedron. Configuration of *RE* sites within the unit cell of (b) 1/1 AC and (c) 2/1 AC. Spheres with different colors in (c) represent *RE* sites with five distinct symmetries, among which RE_1-RE_4 atoms occupy the icosahedron vertices and RE_5 atoms locate on the body-diagonal axis of acute rhombohedron (AR) units that fill the vacant space in between the RTH clusters.

long-range magnetic orders can be attained at lower electron per atom (e/a) ratios than ∼1.81. Opposed to such e/a guideline, a new Tsai-type 2/1 AC with AFM order has been recently reported in the Ga-Pd-Tb system around the composition of $Ga_{50}Pd_{35.5}Tb_{14.5}$ [19] where e/a equals 1.93, marking the first ternary magnetically ordered Tsai-type compound with relatively large e/a. This was later followed by a comprehensive research performed by the present authors aiming to clarify phase stability and atomic structure of the Ga-Pd-*RE* (*RE* = Gd, Tb, Dy, and Ho) ACs [31,32]. The results revealed the possibility of obtaining 1/1 and 2/1 ACs with the same compositions by just altering the annealing temperature. Such a possibility provided a unique opportunity to study the effect of structural evolution towards quasiperiodicity on the physical properties of Ga-Pd-based ACs.

As such, the present study set out to assess the effect of not only atomic structure but also the *RE* type on the magnetic properties of Ga-Pd-*RE* (*RE* = Gd, Tb, Dy, and Ho) 1/1 and 2/1 ACs. This paper is among a few published works comparing magnetic behaviors of lower- and higher-order ACs and/or *i*QCs, which is a prerequisite for understanding the nature of magnetism in quasiperiodic structures. For example, Wang *et al.* [33] compared magnetic properties of SG $Ag_{50}In_{36}Gd_{14}$ *i*QC and 1/1 AC using dc and ac magnetic susceptibility. They reported one-stage freezing of Gd spins at T_f (freezing temperature) = 4.3 K in $Ag_{50}In_{36}Gd_{14}$ *i*QC but two-stage freezing phenomenon in the 1/1 AC with the same composition at $T_{f1} = 3.7$ K and $T_{f2} = 2.4$ K. In a different study [34], magnetic properties of Au-Al-Tm *i*QC and 1/1 AC were compared and SG-like behavior was reported for both compounds, although the geometrical frustration parameter was lower in the *i*QC sample. Comparative study of the magnetic properties of Cd-Mg-*RE* (*RE* = Gd, Tb, Dy, Ho, Er, and Tm) *i*QC, 2/1 and 1/1 ACs with SG behavior [6], on the other hand, revealed higher frustration in quasiperiodic structure than periodic ones assumably due to more random *RE*-*RE* distance distribution in *i*QCs.

In this paper, we present experimental results of dc magnetic susceptibility of the Ga-Pd-*RE* (*RE* = Gd, Tb, Dy, and Ho) 1/1 and 2/1 ACs. To confirm the SG state in some of the samples, we performed additional experiments such as ac magnetic susceptibility and metastable spin relaxation (or aging process). During the discussions, we seek to find possible connections between the atomic structure and the observed magnetic properties by referring to the refined structure models of the Ga-Pd-Tb 2/1 and 1/1 ACs provided elsewhere [31]. We will quantitatively analyze the frequency dependence of the spin-freezing temperature (T_f) in each of the studied SG samples based on the Vogel-Fulcher law [28,35], which will be explained in detail within the text. The findings of the paper should shed light on our understanding about the magnetism in aperiodic systems.

II. EXPERIMENT

Polycrystalline alloys with nominal compositions of $Ga_{50}Pd_{36}RE_{14}$ (*RE* = Gd, Tb, Dy, and Ho) were prepared from high-purity elements using arc melting and subsequent

TABLE I. List of analyzed composition (from ICP analysis), experimental Weiss temperature (θ_w), Néel temperature (T_N), freezing temperature (T_f), and effective magnetic moment (μ_{eff}) obtained for Ga-Pd-*RE* (*RE* = Gd, Tb, Dy, and Ho) 2/1 and 1/1 ACs.

AC type	Analyzed composition (ICP)	μ_{eff} (μ_B/RE_{ion})	$\mu_{calc.}$ (μ_B/RE_{ion})	θ_w (K)	T_{f1} (K)	T_{f2} (K)	T_N (K)	$\lvert\theta_w/T_f\rvert$
1/1 AC	$Ga_{50.0}Pd_{35.8}Gd_{14.2}$	8.0 ± 0.1	7.94	-12.72 ± 0.64	2.73			4.65
2/1 AC	$Ga_{50.1}Pd_{35.8}Gd_{14.1}$	8.2 ± 0.1		-13.96 ± 0.93	4.67			2.99
1/1 AC	$Ga_{49.0}Pd_{37.3}Tb_{13.7}$	9.8 ± 0.1	9.72	-10.32 ± 0.89	3.22			3.20
2/1 AC	$Ga_{49.5}Pd_{36.8}Tb_{13.7}$	9.9 ± 0.3		-10.13 ± 1.26	5.78		3.4	1.75
1/1 AC	$Ga_{48.2}Pd_{37.2}Dy_{14.6}$	10.9 ± 0.3	10.63	-6.47 ± 1.36	2.21			2.92
2/1 AC	$Ga_{48.6}Pd_{36.9}Dy_{14.6}$	10.9 ± 0.2		-4.78 ± 1.18	4.18	2.21		1.14
1/1 AC	$Ga_{48.5}Pd_{37.2}Ho_{14.3}$	10.8 ± 0.1	10.58	-2.25 ± 0.84				
2/1 AC	$Ga_{48.3}Pd_{37.2}Ho_{14.5}$	10.6 ± 0.1		-1.53 ± 0.97	3.22[a]			

[a]In Ga-Pd-Ho 2/1 AC, the onset temperature of deviation between ZFC and FC magnetizations is assumed as T_f.

isothermal annealing at $T = 973$ and 1073 K under Ar atmosphere for obtaining 2/1 and 1/1 ACs, respectively. Inductively coupled plasma (ICP) analysis of the samples, as listed in Table I, revealed a fair consistency with the nominal values. Powder x-ray diffraction (Rigaku SmartLab SE x-ray diffractometer) with Cu-K_α radiation was performed for phase identification. The dc magnetic susceptibility of the samples was measured under zero-field cooled (ZFC) and field-cooled (FC) modes using superconducting quantum interference device magnetometer (Quantum Design, MPMS3) in the temperature range from 1.8 to 300 K and external dc fields up to 7×10^4 Oe. Further, ac magnetic susceptibility measurements were carried out under frequencies ranging from 0.1 to 100 Hz in the temperature range of 2−20 K and $H_{ac} = 1$ Oe. The time dependence of the dc magnetic susceptibility (magnetic relaxation experiment) was measured in ZFC mode under 10 Oe for waiting times of $t_w = 100$, 1000, and 5000 s.

III. RESULTS

A. Phase identification

Figures 2(a) [respectively, 2(b)] presents powder XRD patterns of the $Ga_{50}Pd_{36}RE_{14}$ (*RE* = Gd, Tb, Dy, and Ho) compounds annealed at 973 K (respectively, 1073 K) along with the results of Le Bail fittings [36] obtained by assuming the space groups $Pa\bar{3}$ (respectively, $Im\bar{3}$) using the JANA 2006 software suite [37]. The red and black lines in the figure represent calculated (I_{cal}) and measured (I_{obs}) peak intensities, respectively, while the expected Bragg peak positions are shown by blue vertical bars. As shown, the experimental peak positions and their intensities are consistent with the calculation confirming the high purity of the synthesized 1/1 and 2/1 ACs.

B. Magnetic properties (dc susceptibility)

The temperature dependence of dc magnetic susceptibility of the Ga-Pd-*RE* (*RE* = Gd, Tb, Dy, and Ho) 1/1 and 2/1 ACs

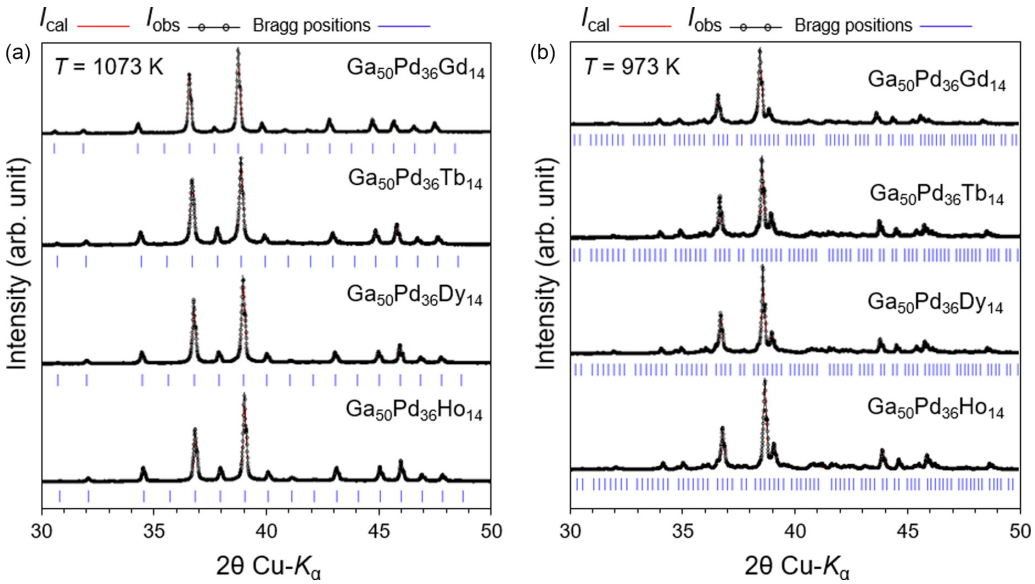

FIG. 2. Le Bail fitting of powder x-ray diffraction (XRD) patterns of the $Ga_{50}Pd_{36}RE_{14}$ (*RE* = Gd, Tb, Dy, and Ho) compounds annealed at (a) 973 and (b) 1073 K. Chemical compositions in the figure are nominal ones. Refer to Table I for the corresponding analyzed compositions.

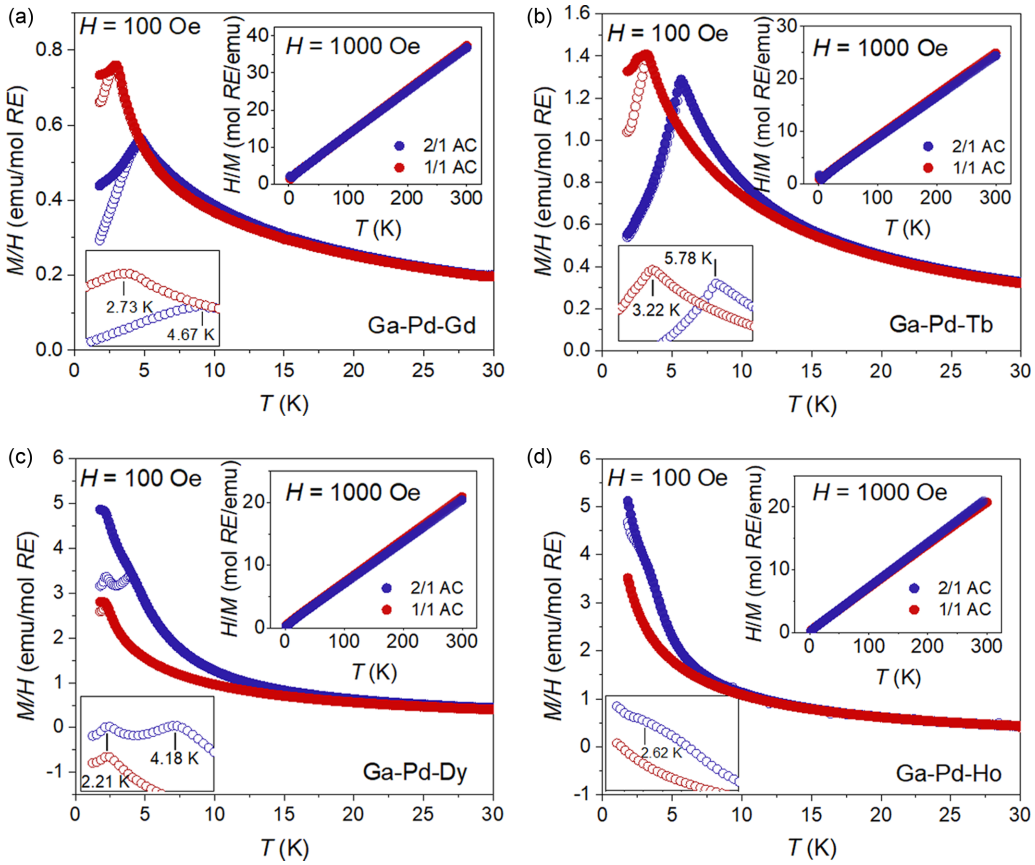

FIG. 3. Temperature dependence of dc magnetic susceptibility of the Ga-Pd-*RE* (*RE* = Gd, Tb, Dy, and Ho) 1/1 and 2/1 ACs under FC and ZFC modes. Insets show corresponding inverse magnetic susceptibility results.

at low temperatures (T = 0–30 K) in FC (filled circles) and ZFC (unfilled circles) modes are shown in the main panels of Fig. 3, where the 1/1 AC (respectively, 2/1 AC) is represented by red (respectively, blue). The high-temperature inverse magnetic susceptibility of all samples in the temperature range of 1.8–300 K (in the upper right insets of Fig. 3) exhibit a linear behavior which can be well fitted to the Curie-Weiss law defined as

$$\chi\,(T) = \frac{N_A \mu_{\rm eff}^2 \mu_B^2}{3k_B(T-\theta_w)} + \chi_0, \qquad (1)$$

where N_A, $\mu_{\rm eff}$, μ_B, k_B, θ_w, and χ_0 denote Avogadro's number, effective magnetic moment, Bohr magneton, the Boltzmann factor, Curie-Weiss temperature (which indicates a sum of all exchange interactions), and the temperature-independent magnetic susceptibility, respectively [38]. The χ_0 equals to almost zero in the present samples. The estimated θ_w (from linear fits to the inverse susceptibility in the temperature range of T = 150–300 K) and $\mu_{\rm eff}$ are listed in Table I. The uncertainty in the estimated values of θ_w and $\mu_{\rm eff}$ in Table I corresponds to fitting the inverse susceptibility data in different temperature ranges within 150 K < T < 300 K. All θ_w values are negative, indicating a dominant AFM exchange interaction between the magnetic moments at high temperatures. The agreement between $\mu_{\rm eff}$ and the theoretical magnetic moments of RE^{3+} free ions defined as $g\sqrt{J(J+1)}\mu_B$ [38] suggests localization of the magnetic moments on RE^{3+} ions.

At low temperatures, most samples except Ga-Pd-Tb 2/1 AC in Fig. 3(b) and Ga-Pd-Ho 1/1 AC in Fig. 3(d) exhibit bifurcation between ZFC and FC curves below T_f, implying SG-like freezing behavior. In the Ga-Pd-Tb 2/1 AC, both FC and ZFC curves display a sharp cusp at T = 5.78 K, suggesting an AFM order establishment. The insets at the bottom-left corners of the main panels in Fig. 3 provide magnified views of the ZFC curves, where the positions of the cusps are more evident. Throughout the paper, the maximum temperature of ZFC magnetization is assumed as T_f (in the SG samples) and a Néel temperature T_N (in the AFM Ga-Pd-Tb 2/1 AC). Notice that the Ho-contained 2/1 AC does not exhibit a maximum but a bifurcation between the FC and ZFC curves at T = 3.22 K. The onset temperature of the deviation is assumed as a T_f due to its nonequilibrium state evidenced by the appearance of frequency-dependent cusp in the ac magnetic susceptibility at the same temperature (which will be discussed later in Fig. 8), as a hallmark of spin-freezing phenomenon [39]. The estimated T_f (or T_N) values are listed in Table I. The establishment of AFM order in the Ga-Pd- Tb 2/1 AC is further confirmed by observing metamagnetic-like anomalies in the field-dependence magnetization curves measured at T = 1.8, 3, and 5 K (all below the transition temperature at T = 5.76 K), as displayed in Fig. 4. The first derivative curves in the inset associated with the maximum slope of the *M*-*H* curves evidence the shift of the anomaly to lower fields (from 0.91 to 0.61 T) as the temperature rises from T = 1.8 to T = 5 K. The occurrence of such anomaly and its shift to

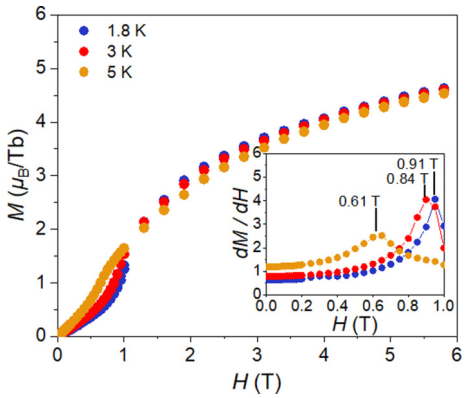

FIG. 4. Magnetization curves of the $Ga_{50}Pd_{36}Tb_{14}$ 2/1 AC as a function of applied magnetic field. The occurrence of metamagnetic-like anomalies is noticed through the maximum slope of the *M*-*H* curve evidenced by sudden peaks in the first derivative curves in the inset. The position of peaks shifts to lower fields (from 0.91 to 0.61 T) as the temperature rises from $T = 1.8$ to $T = 5$ K.

lower fields by increasing temperatures provides supporting evidence that the magnetic transition at $T = 5.76$ K in the $Ga_{50}Pd_{36}Tb_{14}$ 2/1 AC is of AFM type [15].

Figures 5(a) and 5(b) depict the estimated $|\theta_w|$ and T_f (or T_N) versus the de Gennes parameter defined as $dG = (g-1)^2 J(J+1)$, where g and J denote the Landé g factor and the total angular momentum, respectively. The 1/1 and 2/1 ACs are represented by red and blue filled circles, respectively (only AFM Ga-Pd-Tb 2/1 AC is shown by an unfilled circle for distinction). Figure 5(a) evidences approximate proportionality of $|\theta_w|$ to dG, indicating the domination of Ruderman-Kittel-Kasuya-Yosida (RKKY)-type indirect interaction in these compounds [40]. In Fig. 5(b), however, a serious deviation of T_f in Gd-contained ACs from dG scaling, is observed, which is consistent with the previous studies [6,40–43] and is likely to originate from an isotropic behavior of Gd^{3+} ion in the crystalline electric field (CEF). It is a widely held view that the spin-freezing phenomenon in the non-Heisenberg systems is governed by distribution of *RE*-*RE* distances and easy-axis (or plane) directions [28,40]. Since the latter is absent in the Heisenberg systems, their spin-freezing phenomenon is considered to solely arise from the former. Therefore, the present comparative work implies that the absence of local magnetic anisotropy lowers the T_f values. Comprehensive discussion of this subject is provided elsewhere [40,43].

Based on an empirical frustration parameter of $|\theta_w/T_f|$ [33,34,44], the frustration level is about two times lower in the 2/1 ACs than their corresponding 1/1 ACs (see Table I for the $|\theta_w/T_f|$ values). In principle, geometrical frustration arises when the lowest-energy configuration of all two-spin interactions cannot be achieved at the same time due to competition with the neighboring spins. In particular, Tsai-type compounds wherein the *RE* sites form a network of corner-sharing octahedra with the number of nearest-neighbor: $z = 8$ are considered as new type of frustrated magnets. The $|\theta_w/T_c|$ values in Table I indicate a weaker competition between spins in the 2/1 ACs with the space group $Pa\bar{3}$ compared to their corresponding 1/1 ACs with the space group $Im\bar{3}$. Figure 6(a) plots networks of Tb octahedra in the $Ga_{50}Pd_{35.5}Tb_{14.5}$ 1/1 and 2/1 ACs based on the diffraction data obtained from single-crystal x-ray measurement [31]. In Fig. 6(b), the histogram distribution of the edge lengths of an isolated octahedron in the two ACs are compared. As shown, while the octahedron in the 1/1 AC is fairly symmetric, evidenced by two distinct distances at 5.31 and 7.52 Å corresponding to its edges and body diagonals, respectively, the octahedron in the 2/1 AC is quite distorted, evidenced by the widened distances distributed over a range of 0.35–0.55 Å. The appearance of malformed octahedra in the 2/1 AC, which was expected due to the existence of five different symmetrically equivalent *RE* sites in it [see Fig. 1(c)], may partially relieve geometrical frustration inherent to the perfect octahedron spin arrangements provided that the spins are of Ising type.

Another possible contributor to different frustration levels in the 2/1 and 1/1 ACs could be the existence of structural defects such as fractionally occupied sites in the nearest neighbors of *RE* positions in the structure of 1/1 AC that could locally break the mirror symmetry and lead to different CEF

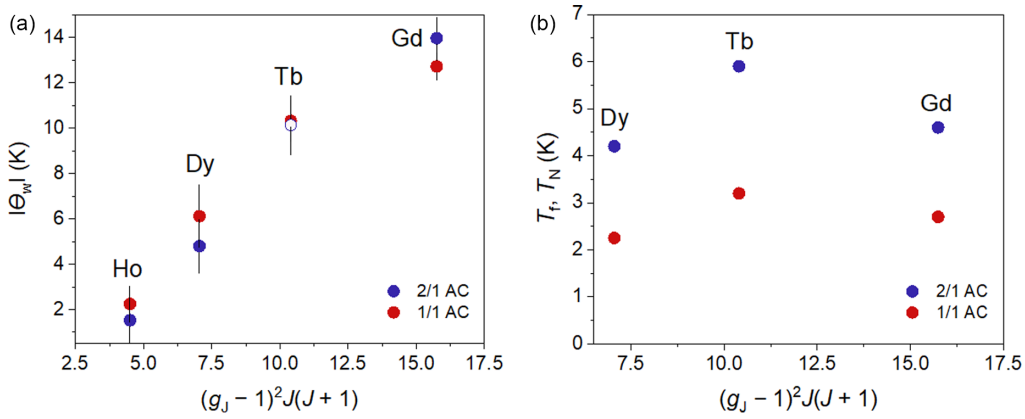

FIG. 5. Variation of (a) $|\theta_w|$ and (b) T_f or T_N as a function of the de Gennes factor: $dG = (g-1)^2 J(J+1)$ for the magnetic 2/1 and 1/1 ACs in the Ga-Pd-*RE* systems. Values related to the AFM Ga-Pd-Tb 2/1 AC are represented by open circles in the figures. Relative correspondence between the experimental $|\theta_w|$ values and the dG of the magnetic *RE* is noticed in all samples. Deviation of T_f in Gd-contained ACs from dG scaling is possibly due to the absence of local magnetic anisotropy in Gd^{3+}.

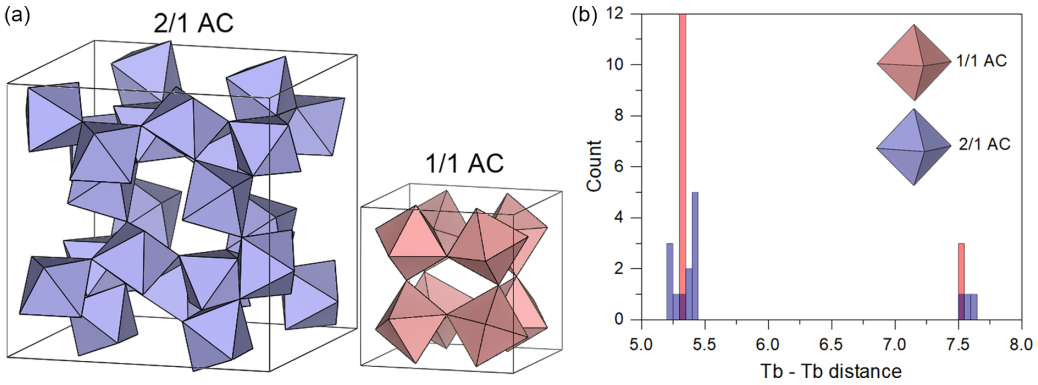

FIG. 6. (a) Network of corner-sharing tilted octahedra in the $Ga_{50}Pd_{35.5}Tb_{14.5}$ 1/1 and 2/1 ACs; (b) histogram distribution of the edge lengths of an isolated octahedron in the two ACs.

potential for different *RE* sites and finally induce frustration. Figure 7 displays refined atomic structures within the nearest neighbor of an isolated Tb^{3+} ion located at (a), (b) icosahedron vertices and (c) along the long body diagonal of the AR in the $Ga_{50}Pd_{35.5}Tb_{14.5}$ (a) 1/1 AC and (b), (c) 2/1 AC. Here, Ga, Pd, and Tb atoms are represented by dark blue, light blue, and red colors, respectively. What stands out in the figure is a significant positional and chemical disorder between Ga and Pd species that occurs on 5 out of 16 vertices of the monocapped, double, pentagonal antiprism polyhedron [see Fig. 7(a)] around Tb^{3+} ions in the 1/1 AC. It can be argued that the localized $4f$ electrons of the Tb^{3+} ions at the center of polyhedron are subject to the point charges of the Ga/Pd on the disordered sites through CEF effect which further induces spin frustration in the 1/1 AC. However, in the 2/1 AC, the vertices of $(Ga : Pd)_{18}Tb$ polyhedron around Tb^{3+} ion on the icosahedron vertices [see Fig. 7(b)] and the AR unit that cages a Tb dimer outside the icosahedron shell [see Fig. 7(c)] are fully occupied by either Ga or Pd atoms forming highly ordered environments, which could be one of the contributing parameters in the establishment of AFM order in the Ga-Pd-Tb 2/1 AC. Note that the estimated frustration parameters in the present compounds are in the range of 1.14–4.65, being comparable to 2.3–3.6 in the ternary Au-Al-Tm [34], and 4.5 in ternary Zn-Mg-Tb [43,45], but lower than 8.7 and 15.5 in the Ag-In-Gd *i*QC and 1/1 AC [33], respectively, and 10 in binary *i*-Cd-Gd [8] systems. By definition, systems with frustration parameter of higher than 10 are classified as strongly frustrated systems [46]; therefore, the present compounds can be considered as weakly frustrated compounds.

C. Magnetic properties (ac susceptibility)

One of the standard experiments to determine "canonical" SG is through the ac magnetic susceptibility measurement [47]. Due to the nonequilibrium nature of SG systems [28], the magnitude and position of their T_f should depend on the measurement frequency (f). Basically, the ac magnetic susceptibility has two components that are related through a relaxation time: in-phase or dispersion (χ'_{ac}) and out-of-phase or absorption (χ''_{ac}) components [28]. In the SG systems, the absorption effect due to the decoupling of spins from the lattice via relaxation process appears as a jump near T_f in the (χ''_{ac}). The main panels in Fig. 8 depict temperature dependence of χ'_{ac} for all samples (except Ga-Pd-Ho 1/1 wherein no anomaly is noticed down to 1.8 K) under f spanning three

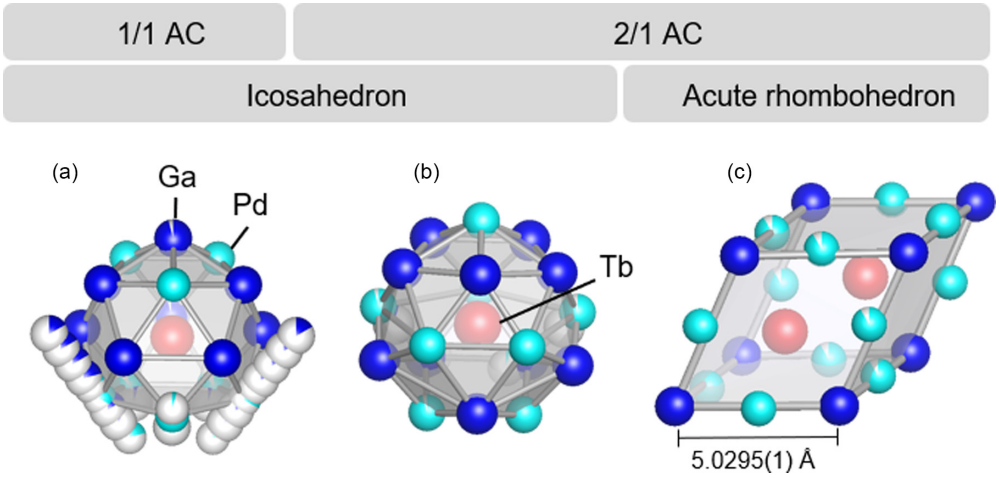

FIG. 7. (a)–(c) Refined atomic structures within the first-nearest neighbor of an isolated Tb^{3+} ion on the (a), (b) icosahedron vertices and (c) along the long-body diagonal of acute rhombohedron in the Ga-Pd-Tb (a) 1/1 AC and (b), (c) 2/1 AC. Ga, Pd, and Tb atoms are represented by dark blue, light blue, and red colors, respectively.

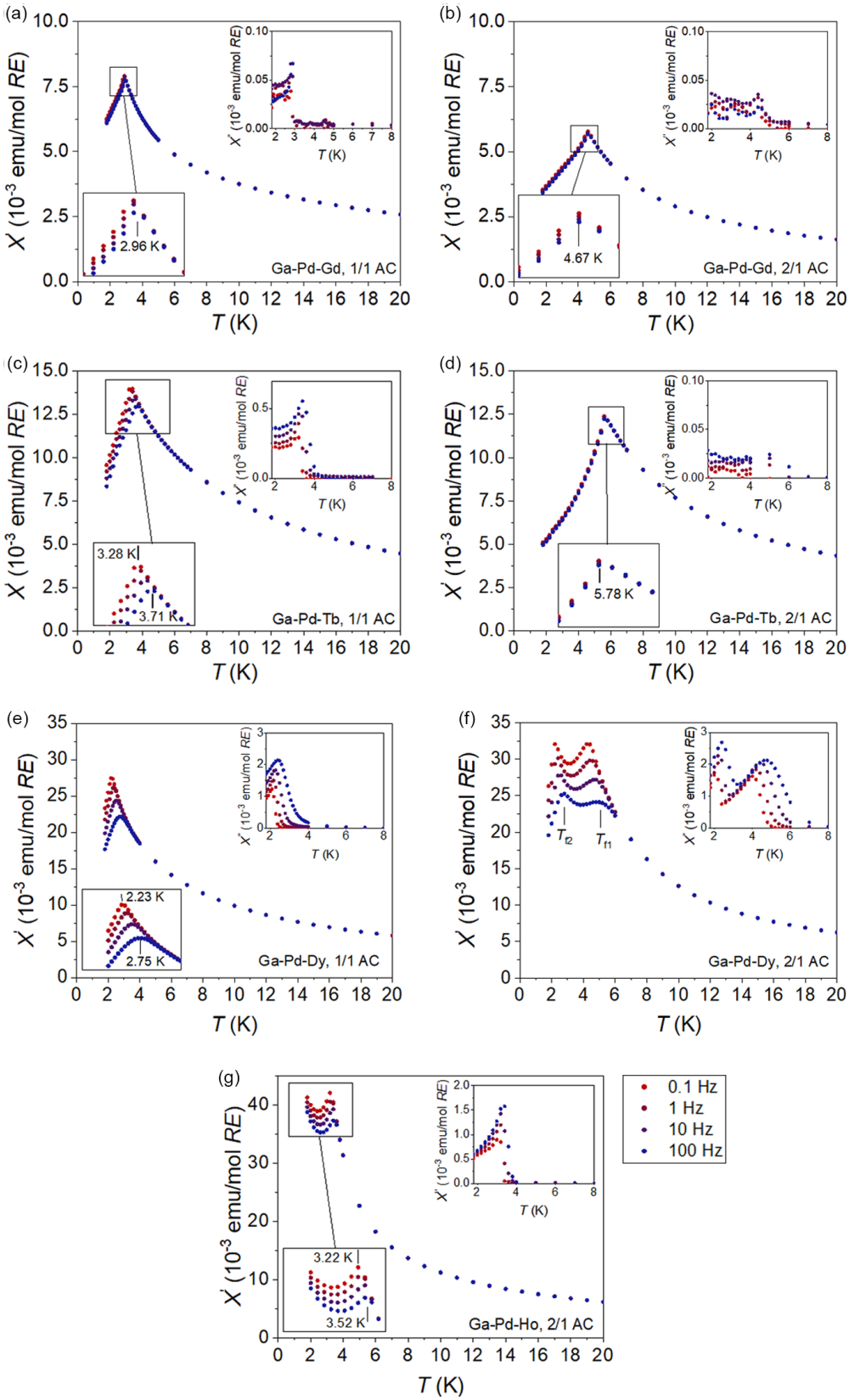

FIG. 8. In-phase component of the ac susceptibility obtained from (a) Ga-Pd-Gd 1/1 AC, (b) Ga-Pd-Gd 2/1 AC, (c) Ga-Pd-Tb 1/1 AC, (d) Ga-Pd-Tb 2/1 AC, (e) Ga-Pd-Dy 1/1 AC, (f) Ga-Pd-Dy 2/1, and (g) Ga-Pd-Ho 2/1 within 1.8 K $< T <$ 20 K under $f_{ac} = 0.1$–100 Hz. Insets represent the corresponding out-of-phase components.

TABLE II. List of experimentally derived T_f, relative change in T_f per decade change in f K, Vogel-Fulcher temperature (T_0), $T_f - T_0$, and activation energy (E_a/k_B) for Ga-Pd-*RE* (*RE* = Gd, Tb, Dy, and Ho) 2/1 and 1/1 ACs.

RE type	1/1 / 2/1 AC	T_f (0.1) (K)	T_f (1) (K)	T_f (10) (K)	T_f (100) (K)	K	T_0 (K)	T_f-T_0 (K)	E_a/k_B
Gd	1/1 AC	2.93	2.95	2.97	2.99	0.006(7)	2.76(5)	0.19(5)	6.47 ± 0.30
	2/1 AC	4.67	4.69	4.71	4.73	0.004(2)	4.43(0)	0.27(0)	5.24 ± 0.18
Tb	1/1 AC	3.28	3.40	3.55	3.71	0.040(2)	1.73(4)	1.76(5)	49.97 ± 1.22
	2/1 AC								
Dy	1/1 AC	2.23	2.36	2.53	2.75	0.049(8)	0.30(6)	2.19(0)	61.62 ± 1.92
	2/1 AC	4.29	4.47	4.71	4.92	0.045(7)	1.96(8)	2.64(5)	75.19 ± 2.31
		2.21	2.36	2.53	2.75	0.074(2)	0.19(2)	2.29(0)	64.63 ± 0.83
Ho	1/1 AC								
	2/1 AC	3.22	3.31	3.42	3.52	0.028(7)	2.11(5)	1.26(3)	35.72 ± 1.51

orders of magnitude from 0.1 to 100 Hz. The corresponding χ''_{ac} are provided in the inset. As shown, χ'_{ac} in the SGs is frequency dependent below T_f even though the level of dependency varies significantly with the *RE* species. At the same time, their corresponding χ''_{ac} rise from a zero background (again by different extents depending on the *RE* type) below T_f. The results, as summarized in Table II, indicate 2–25% shift of T_f in the ACs by three decades variation of f. Figure 9 provides more clear perspective of T_f variation in different *RE*-contained ACs by depicting the normalized T_f (i.e., $T_f/T_{f\,(0.1\,Hz)}$) against f (in logarithmic scale). Take Ga-Pd-Tb 1/1 AC as an example, wherein the position of T_f varies ~15% by three orders of magnitude rise in f. The highest dependency belongs to $Ga_{50}Pd_{36}Dy_{14}$ 2/1 AC [Fig. 8(f)] wherein ~25% shift in the position of T_{f1} is noticed.

On the contrary, Gd-contained ACs [Figs. 8(a) and 8(b)] show the least sensitivity to the change of f as their T_f varies merely by 1−2% despite a clear divergence between their FC and ZFC magnetizations shown in Fig. 3(a). Given that lower response of the Heisenberg SGs (compared to non-Heisenberg ones) to the frequency change has been formerly reported in other alloy systems such as Zn-Mg-*RE* (*RE* = Gd, Tb, and Dy) *i*QCs [48] and even in non–QC-related SGs such as B_{66}*RE* (*RE* = Gd, Tb, Ho, and Er) [49], it seems unlikely to be an inherent nature of the present system. It is rather suggested to arise from magnetic anisotropy (either in easy-axis or plane) energy, i.e., energy of the spin-orbital coupling via CEF, which is about two orders of magnitude smaller in Gd^{3+} with half-filled $4f$ shell than that of typical rare-earth metals [50–54] and thus relatively easier to be overcome during the spin rotation. Strong dependency of χ'_{ac} and χ''_{ac} susceptibilities on magnetic anisotropy and domain-wall energies is a well-acknowledged phenomenon dealt with by a number of theoretical and empirical studies [55–58].

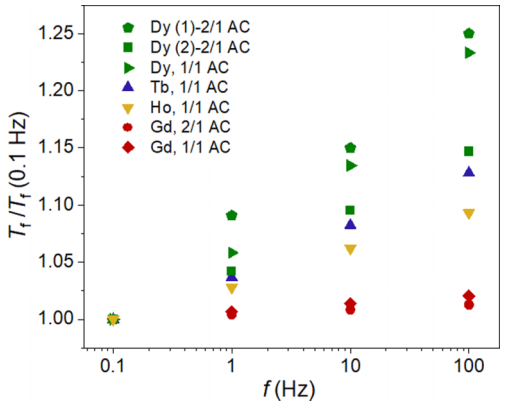

FIG. 9. Normalized T_f by their lowest values obtained at 0.1 Hz vs the measurement f for the present 1/1 and 2/1 ACs.

As further experimental evidence for a glassy behavior in SG samples, ZFC dc magnetization of the samples under probing field of $H = 10$ Oe is recorded at $T = 1.8$ K after different waiting times of $t_w = 100$, 1000, and 5000 s (i.e., aging experiment). Figure 10 shows the magnetization versus t (in logarithmic scale) for all samples. They clearly show time-dependent magnetization characteristic to SG states except the antiferromagnetic Ga-Pd-Tb 2/1 AC. In addition, the dependency of the magnetization on the elapsed time t_w in the SG samples is more evident in the 1/1 ACs than their 2/1 counterparts, assumably due to a pronounced chemical disorder and/or geometrical spin frustration inherent to the perfect *RE* octahedra decoration in the structure of 1/1 ACs, as discussed earlier. Such aging phenomenon is a direct manifestation of the nonequilibrium nature of SG systems, the properties of which should depend on previous history of the system, i.e., waiting times t_w. The Ga-Pd-Tb 2/1 AC, as expected, does not exhibit aging behavior nor time-dependent isothermal magnetization as it is an equilibrium phase.

For a quantitative analysis of the results obtained from the ac magnetic susceptibility measurements, the first step is to calculate a relative change of T_f per decade change in f expressed as $K = \Delta T_f / (T_f \log f)$ for the SG samples, wherein T_f indicates its average value over different frequencies. For Gd-contained 1/1 and 2/1 ACs, the obtained K values, as listed in Table II, are in the range of $0.004(2) < K < 0.006(7)$, which is consistent with typical canonical SG systems such as $Cu_{1-x}Mn_x$ ($K = 0.005$) [28] and a factor of 2 lower than that in the $Ag_{50}In_{36}Gd_{14}$ *i*QC ($K = 0.010$) [33]. For Tb-, Dy-, and Ho-contained SG systems, the obtained K are in the range of 0.028(7)K < 0.074(2), approximately one order of magnitude larger than those in the $Ga_{50}Pd_{36}Gd_{14}$ ACs, about three to seven times larger than those in the $Al_{1-x}Fe_x$ [28] and

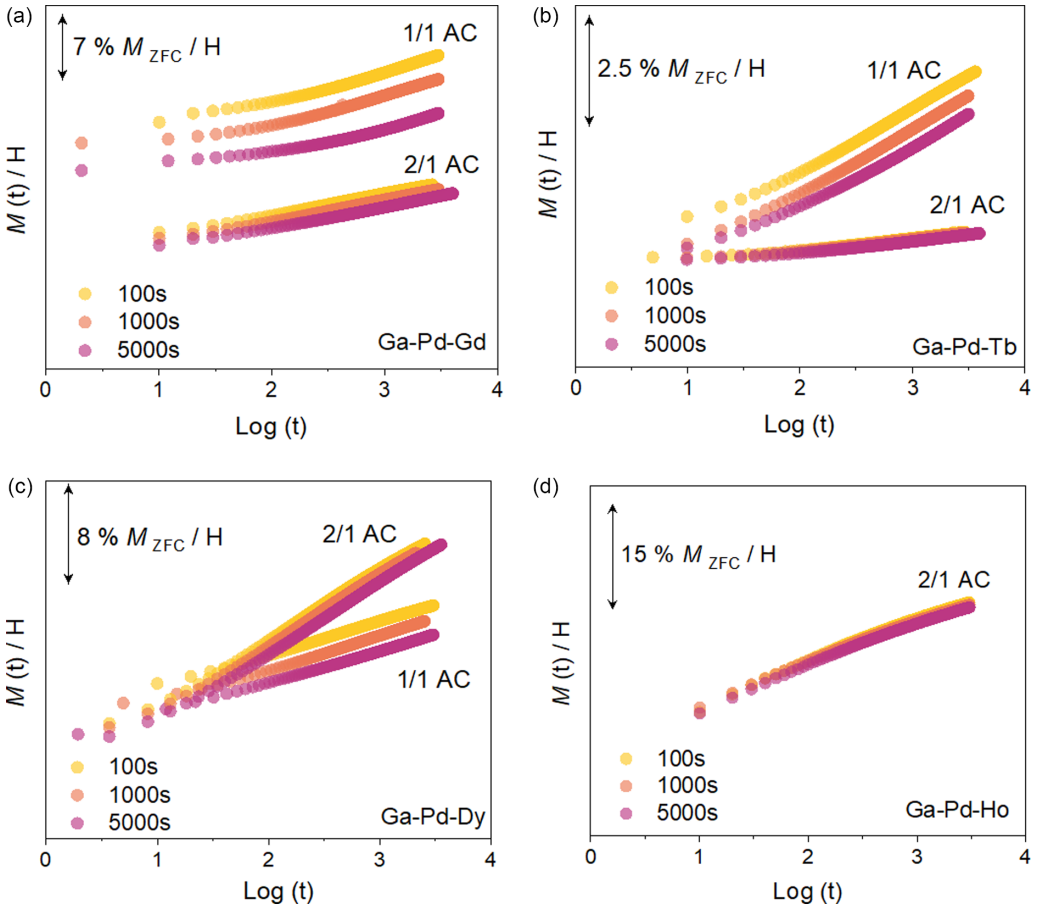

FIG. 10. ZFC magnetization of the Ga-Pd-*RE* (*RE* = Gd, Tb, Dy, and Ho) 1/1 and 2/1 ACs (*RE* = (a) Gd, (b) Tb, (c) Dy, and (d) Ho) after isothermal aging at 1.8 K for different wait times of t_w = 100, 1000, and 5000 s.

$Pd_{1-x}Mn_x$ ($K = 0.013$) [33] SGs, and quite comparable with the $Zn_{57}Mg_{34}Tb_9$ *i*QC ($K = 0.049$) [43]. Basically, the K is a quantitative parameter that reflects the dependency level of T_f to the measurement frequency.

Among the studied samples, the $Ga_{50}Pd_{36}Dy_{14}$ 2/1 AC exceptionally exhibits two distinct anomalies at $T_{f1} = 2.21$ K and $T_{f2} = 4.18$ K with both χ'_{ac} and χ''_{ac} being frequency dependent below T_f [see Fig. 8(f)]. Their shift by three orders of magnitude frequency change reaches up to nearly 25 and 15%, respectively. These features indicate two-stage relaxation process with different characteristic relaxation times, which has also been formerly observed in a number of SG systems such as Ag-In-Gd 1/1 AC [33] and Cd-Mg-Tb 1/1 AC [59], as well as other geometrically frustrated magnets like $Gd_3Ga_5O_{12}$ [60], $Dy_{2-x}Yb_xTi_2O_7$ [61], $Dy_2Ti_2O_7$ [62], and $Fe_{1/4}TiS_2$ [63] and been correlated to formation of different magnetic clusters during the cooling process [63]. Almost a factor of 2 larger $K_1 = 0.071$ compared to $K_2 = 0.044$ in the $Ga_{50}Pd_{36}Dy_{14}$ 2/1 AC indicates that the spin relaxation at T_{f1} is about two times faster than that at T_{f2}. As a direct confirmation of such implication, we measured the time-dependence spin relaxation (also called an aging process [28]) in the $Ga_{50}Pd_{36}Dy_{14}$ 2/1 AC at 1.8 K (below $T_{f1} = 2.21$ K), at 3.2 K (above $T_{f1} = 2.21$ K and below $T_{f2} = 4.18$ K), at 5.2, and 10 K (both above T_{f1} and T_{f2}) under 10 Oe. The results are shown in Fig. 11, wherein the normalized dc ZFC magnetization, i.e., $M(t)/M(t = 0)$, is depicted. Clearly, the magnetization at 1.8 K is less dependent on time than that at 3.2 K and is almost independent from time at 5.2 and 10 K, confirming different spin dynamics at each freezing stage in the $Ga_{50}Pd_{36}Dy_{14}$ 2/1 AC.

A final step for safe conclusion of SG state is to rule out the possibility of superparamagnet-type blocking in the present

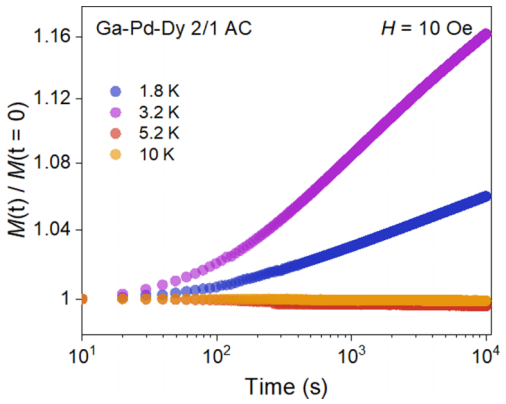

FIG. 11. Variation of the normalized dc magnetization $M(t)/M(t = 0)$ in ZFC mode vs time in logarithmic scale measured for the Ga-Pd-Dy 2/1 AC at 1.8, 3.2, 5.2, and 10 K under 10 Oe.

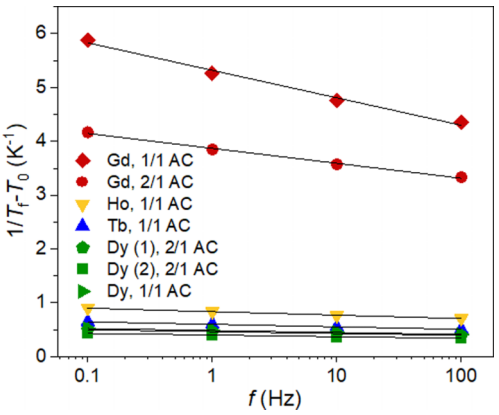

FIG. 12. Variation of $1/(T_f–T_0)$ in the SG samples including 1/1 and 2/1 ACs as a function of measuring frequency f.

samples. One of the quantitative approaches in this direction is to fit the frequency-dependence T_f data to the following Arrhenius law:

$$f = f_0 \exp\left[-\frac{E_a}{k_B(T)}\right], \tag{2}$$

where f denotes the driving frequency of the ac measurement and T, for our purpose, is considered as T_f. The best fitting of the data to Eq. (2) yields completely unphysical values such as $f_0 = 10^{142}$ Hz and $E_a/k_B = 1009.4$ K, as in the case of Ga-Pd-Tb 1/1 AC. The emergence of such unphysical fitting values, indeed, distinguishes the present SGs from superparamagnets where the Arrhenius law holds true [47]. The alternative approach for fitting the frequency dependence of T_f data is based on an empirical Vogel-Fulcher law which describes the viscosity of supercooled liquids in real glasses [28,35,64]. The Vogel-Fulcher law is described as below:

$$f = f_0 \exp\left[-\frac{E_a}{k_B(T_f - T_0)}\right], \tag{3}$$

where the f_0, E_a, and T_0 are fitting parameters. The latter is referred to as an "ideal glass temperature" in real glasses but in SGs, it is commonly considered as a measure of intercluster interaction strength [28] given that SG is a collection of interacting magnetic clusters after all. Some [35], however, correlate T_0 to a real temperature where an underlying phase transition, for which the T_f obtained from dc measurement is just a dynamic manifestation, takes place. By assuming $f_0 = 1\times10^{13}$ Hz, as a typical value in SG systems [35], the best fit of the T_f (f) to Eq. (3) results in E_a/k_B and T_0 values listed in Table II. As seen, the T_0 in each compound is always lower than the corresponding T_f, which is a logical outcome if T_0 is considered as a real transition temperature. Figure 12 depicts variation of $1/(T_f–T_0)$ versus f (in logarithmic scale), wherein a linear correspondence between the two is clear. Using the Vogel-Fulcher law, therefore, allows a reasonable interpretation of the frequency dependence of T_f with physical fitting parameters. Based on a number of reports [33,35,43,64–66], the fitting parameters E_a/k_B and T_0 can further be used to derive more information about the nature of SG. It has been proposed that in SGs with strong RKKY-type interaction, the $T_f - T_0 \ll T_f$ condition is satisfied, while for those with a weak dominance of RKKY interaction, one could expect $T_0 \ll T_f$. In the present ACs, the T_f–T_0 values are in a range of $0.19(5) - 0.27(0)$ in the Gd-contained ACs, 1.76(5) in the Tb-contained 1/1 AC, $2.19(0) - 2.64(5)$ in the Dy-contained ACs, and 1.26(3) in the Ho-contained 2/1 AC. These values satisfy the $T_f - T_0 \ll T_f$ condition in the Gd-contained ACs where the strong RKKY-type interaction is expected. For the non-Heisenberg SGs, though, $T_0 \ll T_f$ is satisfied, implying a weak dominance of RKKY interaction mediated by itinerant electrons, which is also the case in Al-Pd-Mn *i*QC [64]. Note that the same approach has already been applied on some *i*QCs and ACs with SG behavior [33,43,64,66].

IV. CONCLUSION

In the present paper, we investigated magnetic properties of the Ga-Pd-*RE* (*RE* = Gd, Tb, Dy, and Ho) 1/1 and 2/1 ACs in detail. The magnetic susceptibilities (both dc and ac) evidenced SG-like freezing behavior for most of the studied samples except for Ga-Pd-Tb 2/1 AC and Ga-Pd-Ho 1/1 AC. In the former, a long-range AFM order is noticed at 5.78 K. The empirical frustration parameter $|\theta_w/T_f|$ indicated lower frustration levels in the 2/1 ACs compared with their corresponding 1/1 ACs. This phenomenon was partly correlated to the malformed octahedron arrangement of *RE* sites and disorder-free environment in their nearest neighbor in the 2/1 ACs. The ac magnetic susceptibility results showed the least sensitivity of the Gd-contained SGs (Heisenberg systems) to the frequency change, while non-Heisenberg ones were very much responsive. This phenomenon was associated with the relatively weak energy of the spin-orbital coupling via CEF in Gd^{3+} making it easier to be overcome during the spin rotation. Furthermore, the frequency dependence of T_f in SG samples was explained by means of the Vogel-Fulcher law.

As for the future work, one may consider performing comparative and systematic investigation on aging, relaxation, and rejuvenation in Heisenberg and non-Heisenberg SGs.

ACKNOWLEDGMENTS

This work was supported by Japan Society for the Promotion of Science through Grants-in-Aid for Scientific Research (Grants No. JP19H05817, No. JP19H05818, No. JP19H05819, and No. JP21H01044) and JST, CREST Grant No. JPMJCR22O3, Japan.

[1] D. Shechtman, I. Blech, D. Gratias, and J. W. Cahn, Metallic Phase with Long-Range Orientational Order and No Translational Symmetry, Phys. Rev. Lett. **53**, 1951 (1984).

[2] M. Duneau and A. Katz, Quasiperiodic Patterns, Phys. Rev. Lett. **54**, 2688 (1985).

[3] H. Takakura, C. P. Gómez, A. Yamamoto, M. De Boissieu, and A. P. Tsai, Atomic structure of the binary icosahedral Yb–Cd quasicrystal, Nat. Mater. **6**, 58 (2006).

[4] A. I. Goldman and R. F. Kelton, Quasicrystals and crystalline approximants, Rev. Mod. Phys. **65**, 213 (1993).

[5] T. Yamada, N. Fujita, and F. Labib, 2/1 and 1/1 cubic approximants in the ternary R-Cd-Mg (R = Y, Er) systems, Acta Cryst. B **77**, 638 (2021).

[6] F. Labib, D. Okuyama, N. Fujita, T. Yamada, S. Ohhashi, T. J. Sato, and A.-P. Tsai, Magnetic properties of icosahedral quasicrystals and their cubic approximants in the Cd–Mg–RE (*RE* = Gd, Tb, Dy, Ho, Er, and Tm) systems, J. Phys.: Condens. Matter **32**, 415801 (2020).

[7] A. I. Goldman, Magnetism in icosahedral quasicrystals: Current status and open questions, Sci. Technol. Adv. Mater. **15**, 044801 (2014).

[8] A. I. Goldman, T. Kong, A. Kreyssig, A. Jesche, M. Ramazanoglu, K. W. Dennis, S. L. Bud'ko, and P. C. Canfield, A family of binary magnetic icosahedral quasicrystals based on rare earths and cadmium, Nat. Mater. **12**, 714 (2013).

[9] K. Inagaki, S. Suzuki, A. Ishikawa, T. Tsugawa, F. Aya, T. Yamada, K. Tokiwa, T. Takeuchi, and R. Tamura, Ferromagnetic 2/1 quasicrystal approximants, Phys. Rev. B **101**, 180405(R) (2020).

[10] A. Ishikawa, T. Hiroto, K. Tokiwa, T. Fujii, and R. Tamura, Composition-driven spin glass to ferromagnetic transition in the quasicrystal approximant Au-Al-Gd, Phys. Rev. B **93**, 024416 (2016).

[11] T. Hiroto, K. Tokiwa, and R. Tamura, Sign of canted ferromagnetism in the quasicrystal approximants Au-SM-R (SM = Si, Ge and Sn/R = Tb, Dy and Ho), J. Phys.: Condens. Matter **26**, 216004 (2014).

[12] G. Gebresenbut, M. S. Andersson, P. Beran, P. Manuel, P. Nordblad, M. Sahlberg, and C. P. Gomez, Long range ordered magnetic and atomic structures of the quasicrystal approximant in the Tb-Au-Si system, J. Phys.: Condens. Matter **26**, 322202 (2014).

[13] T. Hiroto, G. H. Gebresenbut, C. Pay Gómez, Y. Muro, M. Isobe, Y. Ueda, K. Tokiwa, and R. Tamura, Ferromagnetism and re-entrant spin-glass transition in quasicrystal approximants Au-Sm-Gd (SM = Si, Ge), J. Phys.: Condens. Matter **25**, 426004 (2013).

[14] R. Tamura, A. Ishikawa, S. Suzuki, A. Kotajima, Y. Tanaka, N. Shibata, T. Yamada, T. Fujii, C. Wang, M. Avdeev, K. Nawa, D. Okuyama, and T. J. Sato, Experimental observation of long-range magnetic order in icosahedral quasicrystals, J. Am. Chem. Soc. **143**, 19938 (2021).

[15] R. Tamura, Y. Muro, T. Hiroto, K. Nishimoto, and T. Takabatake, Long-range magnetic order in the quasicrystalline approximant Cd6Tb, Phys. Rev. B **82**, 220201(R) (2010).

[16] D. H. Ryan, J. M. Cadogan, T. Kong, P. C. Canfield, A. I. Goldman, and A. Kreyssig, A neutron diffraction demonstration of long-range magnetic order in the quasicrystal approximant DyCd6, AIP Adv. **9**, 035312 (2019).

[17] A. Ishikawa, T. Fujii, T. Takeuchi, T. Yamada, Y. Matsushita, and R. Tamura, Antiferromagnetic order is possible in ternary quasicrystal approximants, Phys. Rev. B **98**, 220403(R) (2018).

[18] T. J. Sato, A. Ishikawa, A. Sakurai, M. Hattori, M. Avdeev, and R. Tamura, Whirling spin order in the quasicrystal approximant Au72Al14Tb14, Phys. Rev. B **100**, 054417 (2019).

[19] Y. G. So, K. Takagi, and T. J. Sato, Formation and magnetic properties of Ga-Pd-Tb 2/1 approximant, J. Phys.: Conf. Ser. **1458**, 012003 (2020).

[20] S. Yoshida, S. Suzuki, T. Yamada, T. Fujii, A. Ishikawa, and R. Tamura, Antiferromagnetic order survives in the higher-order quasicrystal approximant, Phys. Rev. B **100**, 180409(R) (2019).

[21] A. Jagannathan, Quantum Spins and Quasiperiodicity: A Real Space Renormalization Group Approach, Phys. Rev. Lett. **92**, 047202 (2004).

[22] S. Thiem and J. T. Chalker, Long-range magnetic order in models for rare-earth quasicrystals, Phys. Rev. B **92**, 224409 (2015).

[23] S. Matsuo, S. Fujiwara, H. Nakano, and T. Ishimasa, Long range antiferromagnetic order in Ising model simulations in a two-dimensional Penrose lattice, J. Non. Cryst. Solids **334&335**, 421 (2004).

[24] E. Y. Vedmedenko, U. Grimm, and R. Wiesendanger, Noncollinear Magnetic Order in Quasicrystals, Phys. Rev. Lett. **93**, 076407 (2004).

[25] S. Thiem and J. T. Chalker, Magnetism in rare-earth Quasicrystals: RKKY interactions and ordering, Europhys. Lett. **110**, 17002 (2015).

[26] C. Godréche, J. M. Luck, and H. Orland, Magnetic phase structure on the Penrose lattice, J. Stat. Phys. **45**, 777 (1986).

[27] R. Lifshitz, Symmetry of Magnetically Ordered Quasicrystals, Phys. Rev. Lett. **80**, 2717 (1998).

[28] J. A. Mydosh, *Spin Glasses: An Experimental Introduction* (Taylor & Francis, London, 1993).

[29] T. Kong, S. L. Budko, A. Jesche, J. McArthur, A. Kreyssig, A. I. Goldman, and P. C. Canfield, Magnetic and transport properties of I-R-Cd icosahedral quasicrystals (R = Y, Gd-Tm), Phys. Rev. B B**90**, 014424 (2014).

[30] S. Suzuki, A. Ishikawa, T. Yamada, T. Sugimoto, A. Sakurai, and R. Tamura, Magnetism of Tsai-type quasicrystal approximants, Mater. Trans. **62**, 298 (2021).

[31] F. Labib, H. Takakura, A. Ishikawa, and R. Tamura (unpublished).

[32] F. Labib, A. Ishikawa, and R. Tamura (unpublished).

[33] P. Wang, Z. M. Stadnik, K. Al-Qadi, and J. Przewoźnik, A comparative study of the magnetic properties of the 1/1 approximant $Ag_{50}In_{36}Gd_{14}$ and the icosahedral quasicrystal $Ag_{50}In_{36}Gd_{14}$, J. Phys.: Condens. Matter **21**, 436007 (2009).

[34] M. Nakayama, K. Tanaka, S. Matsukawa, K. Deguchi, K. Imura, T. Ishimasa, and N. K. Sato, Localized electron magnetism in the icosahedral Au-Al-Tm quasicrystal and crystalline approximant, J. Phys. Soc. Jpn. **84**, 5 (2015).

[35] J. L. Tholence, On the frequency dependence of the transition temperature in spin glasses, Solid State Commun. **88**, 917 (1993).

[36] A. Le Bail, H. Duroy, and J. L. Fourquet, Ab-initio structure determination of LiSbWO6 by x-ray powder diffraction, Mater. Res. Bull. **23**, 447 (1988).

[37] V. Petrícek, M. Dušek, and L. Palatinus, Crystallographic computing system JANA2006: General features, Z. Kristallogr. **229**, 345 (2014).

[38] S. Blundell, *Magnetism in Condensed Matter Physics*, 1st ed. (Oxford University Press, New York, 2001).

[39] J. A. Mydosh, Disordered magnetism and spin glasses, J. Magn. Magn. Mater. **157-158**, 606 (1996).

[40] P. C. Canfield and I. R. Fisher, $R_9Mg_{34}Zn_{57}$ icosahedral quasicrystals: The tuning of a model spin glass, J. Alloys Compd. **317-318**, 443 (2001).

[41] S. E. Sebastian, T. Huie, I. R. Fisher, K. W. Dennis, and M. J. Kramer, Magnetic properties of single grain R-Mg-Cd primitive icosahedral quasicrystals (R = Y, Gd, Tb or Dy), Philos. Mag. **84**, 1029 (2004).

[42] I. R. Fisher, Z. Islam, J. Zarestky, C. Stassis, M. J. Kramer, A. I. Goldman, and P. C. Canfield, Magnetic properties of icosahedral R-Mg-Zn quasicrystals (R = Y, Tb, Dy, Ho and Er), J. Alloys Compd. **303-304**, 223 (2000).

[43] I. R. Fisher, K. O. Cheon, A. F. Panchula, P. C. Canfield, M. Chernikov, H. R. Ott, and K. W. Dennis, Magnetic and transport properties of single-grain R-Mg-Zn icosahedral quasicrystals [R = Y, (Y1-XGdx), (Y1-XTbx), Tb, Dy, Ho, and Er], Phys. Rev. B **59**, 308 (1999).

[44] T. J. Sato, J. Guo, and A. P. Tsai, Magnetic properties of the icosahedral Cd-Mg-rare-earth quasicrystals, J. Phys.: Condens. Matter **13**, L105 (2001).

[45] Y. Hattori, A. Niikura, A. P. Tsai, A. Inue, T. Masumoto, K. Fukamichi, H. Aruga-Katori, and T. Goto, Spin-glass behaviour of icosahedral Mg-Gd-Zn and Mg-Tb-Zn quasi-crystals, J. Phys.: Condens. Matter **7**, 2313 (1995).

[46] K. H. J. Buschow, *Handbook of Magnetic Materials* (Elsevier, Amsterdam, 2001), Vol. 13.

[47] J. A. Mydosh, Spin glasses: Redux: An updated experimental/materials survey, Rep. Prog. Phys. **78**, 052501 (2015).

[48] S. L. Bud'Ko and P. C. Canfield, Frequency dependence of the spin glass freezing temperatures in icosahedral r–Mg–Zn (R = rare earth) quasicrystals, Philos. Mag. **92**, 4492 (2012).

[49] H. Kim, S. L. Bud'ko, M. A. Tanatar, D. V. Avdashchenko, A. V. Matovnikov, N. V. Mitroshenkov, V. V. Novikov, and R. Prozorov, Magnetic properties of RB66 (R = Gd, Tb, Ho, Er, and Lu), J. Supercond. Nov. Magn. **25**, 2371 (2012).

[50] M. Colarieti-Tosti, S. I. Simak, R. Ahuja, L. Nordström, O. Eriksson, D. Åberg, S. Edvardsson, and M. S. S. Brooks, Origin of Magnetic Anisotropy of Gd Metal, Phys. Rev. Lett. **91**, 157201 (2003).

[51] T. Sawano, Y. Shinagawa, T. Shiino, K. Imura, K. Deguchi, and N. K. Sato, Pressure effects on Ce-based Kondo approximant crystal, AIP Adv. **8**, 4 (2018).

[52] X. C. Kou, T. S. Zhao, R. Grössinger, and F. R. De Boer, ac-susceptibility anomaly and magnetic anisotropy of R2Co17 Compounds, with R = Y, Ce, Pr, Nd, Sm, Gd, Tb, Dy, Ho, Er, Tm, and Lu, Phys. Rev. B **46**, 6225 (1992).

[53] K. Enpuku, S. Draack, F. Ludwig, and T. Yoshida, Evaluation of effective magnetic anisotropy constant of magnetic nanoparticles from coercive field of AC magnetization curve, J. Appl. Phys. **130**, (2021).

[54] W. D. Corner, D. M. Paige, R. D. Hawkins, D. Fort, and D. W. Jones, Magnetocrystalline anisotropy of Gd/Tb alloys, J. Magn. Magn. Mater. **51**, 89 (1985).

[55] J. Schreiber and D. Schulz, Magnetic relaxation in the Heisenberg spin glass, Phys. Status Solidi **145**, 695 (1988).

[56] J. P. Bouchaud, V. Dupuis, J. Hammann, and E. Vincent, Separation of time and length scales in spin glasses: Temperature as a microscope, Phys. Rev. B **65**, 024439 (2001).

[57] B. Frietsch, J. Bowlan, R. Carley, M. Teichmann, S. Wienholdt, D. Hinzke, U. Nowak, K. Carva, P. M. Oppeneer, and M. Weinelt, Disparate ultrafast dynamics of itinerant and localized magnetic moments in gadolinium metal, Nat. Commun. **6**, 8262 (2015).

[58] C. V. Topping and S. J. Blundell, A.C. susceptibility as a probe of low-frequency magnetic dynamics, J. Phys.: Condens. Matter **31**, 013001 (2019).

[59] F. Labib, D. Okuyama, N. Fujita, T. Yamada, S. Ohhashi, D. Morikawa, K. Tsuda, T. J. Sato, and A. P. Tsai, Structural-transition-driven antiferromagnetic to spin-glass transition in Cd–Mg–Tb 1/1 approximants, J. Phys.: Condens. Matter **32**, 485801 (2020).

[60] P. Schiffer, A. P. Ramirez, D. A. Huse, P. L. Gammel, U. Yaron, D. J. Bishop, and A. J. Valentino, Bulk Quantum Efficiency in Indium Antimonide, Phys. Rev. Lett. **74**, 2379 (1995).

[61] G. Ehlers, A. L. Cornelius, T. Fennell, M. Koza, S. T. Bramwell, and J. S. Gardner, Evidence for two distinct spin relaxation mechanisms in "hot" spin ice Ho2Ti2O7, J. Phys.: Condens. Matter **16**, S635 (2004).

[62] J. Snyder, S. Slusky, R. J. Cava, and P. Schiffer, Dirty spin ice: The effect of dilution on spin freezing in Dy2Ti2O7, Phys. Rev. B **66**, 064432 (2002).

[63] M. Koyano, M. Suezaea, W. Hajime, and M. Inoue, Low-field magnetization and AC magnetic susceptibility of spin- and cluster-glasses of itinerant magnet FexTiS2, J. Phys. Soc. Jpn. **63**, 1114 (1994).

[64] M. A. Chernikov, A. Bernasconi, C. Beeli, A. Schilling, and H. R. Ott, Low-temperature magnetism in icosahedral $Al_{70}Mn_9Pd_{21}$, Phys. Rev. B **48**, 3058 (1993).

[65] C. N. Guy, J. L. Tholence, H. Maletta, D. J. Thouless, J. A. Hertz, and S. Kirkpatrick, Panel discussion: Spin glasses, J. Appl. Phys. **50**, 7308 (1979).

[66] P. Kozelj, S. Jazbec, S. Vrtnik, A. Jelen, J. Dolinsek, M. Jagodic, Z. Jaglicic, P. Boulet, M. C. de Weerd, J. Ledieu, J. M. Dubois, and V. Fournée, Geometrically frustrated magnetism of spins on icosahedral clusters: The $Gd_3Au_{13}Sn_4$ quasicrystalline approximant, Phys. Rev. B **88**, 214202 (2013).